EMR-based Switched Model of DC Railway Systems Supplied by Reversible Traction Power Substations and Regenerative Trains

C. Mayet[1], A. Bouscayrol[2], P. Arboleya[3], P. Delarue[2], B. Mohamed[3], and I. El-Sayed[3]

1. SATIE – UMR CNRS 8020, Conservatoire National des Arts et Métiers, ENS Paris-Saclay, F-75003 Paris, France
2. Univ. Lille1, Centrale Lille, Arts et Métiers Paris Tech, HEI, EA 2697 – L2EP – Laboratoire d'Electrotechnique et d'Electronique de Puissance, F-59000 Lille, France
3. LEMUR Research Group, University of Oviedo, Gijon Campus, Asturias 33204 Gijon, Spain
Contact author: clement.mayet@lecnam.net

***Abstract*—Simulation tools are essential for designing and sizing the infrastructure and operation of electrical railway systems. With the advent of innovative solutions to save energy, the accuracy of estimates of energy consumptions and voltages must be increased, while keeping fast computing capabilities. Due to the numerous non-linearities of this kind of system, complex iterative solvers are often used. However, a new simulation technique based on switched models for the different subsystems has recently been developed for conventional DC traction systems with non-reversible traction power substations (TPS). This technique avoids the use of complex numerical solvers. This paper extends this simulation approach to include reversible TPS using Energetic Macroscopic Representation (EMR). Simulations are carried out and an energy saving of 7 % on the total energy consumption is allowed by the reversible TPS for the studied case.**

Keywords—DC Traction System, Reversible Traction Power Substation, Switched Models, Modified Nodal Analysis, Energetic Macroscopic Representation (EMR).

I. INTRODUCTION

Nowadays, electric public transport systems are key players in facing the current challenges in terms of energy savings and greenhouse gas emissions [1]. For this reason, DC traction system are used intensively in dense urban area due to their high performances and low polluting emissions. Currently, new solutions are more and more studied and developed to further improve the overall efficiency [2]. For example, on-board or wayside energy storage systems [3]-[7] (ESS) or reversible Traction Power Substations (TPS) [6]-[8] can be used to save braking energy. However, these technologies induce additional costs and complexity. Their effectiveness must therefore be evaluated before their real implementations.

Numerous models and simulation tools have been proposed in the last decades to estimate the potential energy savings of DC railway systems [4], [6], [9], [10]. Complex power flow solvers have therefore been developed to take into account the dynamic variation of the topology of the DC Traction Network (DCTN) (due to the movement of the trains) and the non-linear behaviors of the different subsystems. The dynamic variation of the topology of the DCTN is resolved by updating the DCTN model at each simulation time according to the positions of each subsystem. Non-linear behaviors are generally solved using numerical iterative solvers. Most existing tools use the conductance matrix iterative approach known as the Current Injection (CI) method, which iteratively determines the equivalent currents of each subsystem connected to the DCTN [9], [10]. The CI is then coupled with a Modified Nodal Analysis (MNA) to solve the entire DC railway system [11], [12]. Algebraic equations with iterative methods, such as Newton-Raphson, Point-Jacobi, or Zollekopf's bifactorisation and incomplete Cholesky conjugate gradient methodologies are then necessary for convergence. The objective of these solvers is to adapt the non-linear behaviors of the different subsystems with the limited receptivity of the DCTN. The receptivity is limited by the voltage increase due to the resistive part of the DCTN, and by the non-reversible TPS, which act as equivalent capacitors when they are blocked. The main non-linear behaviors are the overvoltage protection of regenerative trains [13], the non-reversibility of diode rectifiers (TPS) [14], and the controls of the reversible TPS and ESS [6]-[8]. Innovative solutions therefore require improving models and solvers for better estimations of the power flows and voltages.

Recently, the authors have proposed switched models for the train (to take into account the overvoltage protection) and for the conventional TPS (to take into account the non-linearity of the diode rectifier) [15]. This approach is perfectly capable of simulating the studied system with high accuracy of the results on the estimations of power flows, DC voltages, and energy consumption. In addition, the developed approach does not need a numerical iterative solver for convergence and is fast to compute. The proposed approach can therefore be used for designing, sizing, and optimizing new DC railway systems.

The objective of this paper is to extend the switched model approach to reversible TPS. The Energetic Macroscopic Representation (EMR) is used as common representation tool [16]. Section II presents the models of the different subsystems of DC railway systems (trains, TPS, DCTN). Then, Section III develops the simulation procedure of the whole studied system. Section IV presents the simulation results with non-reversible and reversible TPS. Section V concludes this work.

II. MODELS OF THE DIFFERENT SUBSYSTEMS

This section describes the models of the different subsystems of railway systems (Fig. 1). They are composed of trains (T), a DC Traction Network (DCTN), and Traction Power Substations (TPS) which can be reversible or not. The TPS converts energy from the AC Distribution Network (ACDN) to the DCTN, and the DCTN supplies the trains along the line using a catenary or a third rail system. All the models are organized using the Energetic Macroscopic Representation (EMR) [16]. EMR is a graphical description tool that highlights the energy properties of complex systems. It organizes the system into interconnected basic elements: source (green oval), accumulation (orange crossed rectangle), mono-physical conversions (orange square) and distribution (orange double square) of energy. Switching elements have been introduced to take into account the non-linearities of the subsystems. All elements are connected according to the action and reaction principle. The product of the action variables with the reaction variables leads to the power exchanged between two elements. All components are described respecting the physical causality (i.e. integral causality).

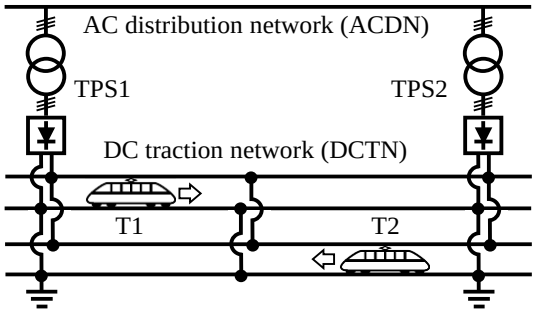

Fig. 1. Typical DC railway system.

A. Model of the Trains

The train model takes into account its different components (Fig. 2) [17]. The connection to the DCTN is made by the pantograph or the third rail. The equipment is supplied through one or several input filter(s) composed of smoothing inductor(s) and DC bus(es). The auxiliaries (Aux.) (lights, compressors, air conditioning, etc.), rheostatic brake, and traction subsystems are connected to the DC bus(es). The traction subsystem consists in inverters, machines, gearboxes, and wheels. The train model determines the current i_{tot}, absorbed or injected, on the DC bus as a function of the power of the auxiliaries p_{aux}, the power of the traction subsystem p_{tr}, and the voltage of the DC bus u_f (1). Traction subsystem and auxiliaries are therefore considered as a current source on the EMR of the train model (Fig. 3).

$$i_{tot} = \frac{p_{aux} + p_{tr}}{u_f} \tag{1}$$

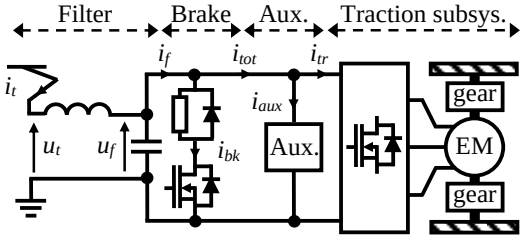

Fig. 2. Equivalent mono-machine train.

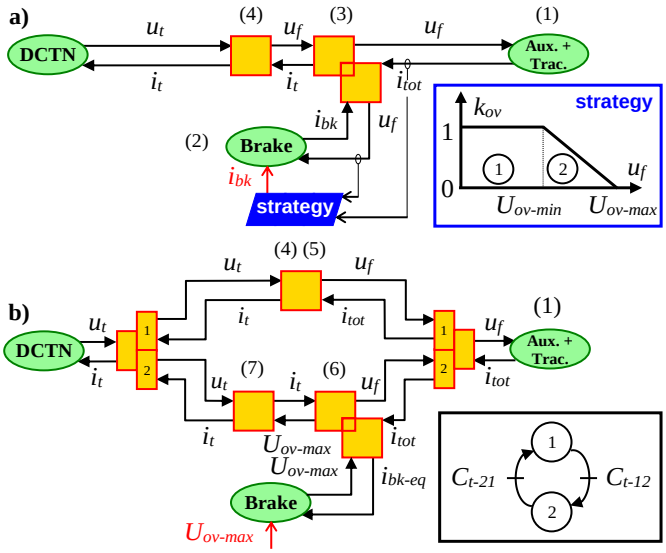

Fig. 3. EMR of the train: a) Conventional model, b) Switched model.

The DCTN imposes the voltage u_t of the catenary or the third rail. During the braking phase, the train recovers the braking energy to the DCTN. However, a rheostatic brake is used to dissipate the braking energy in case of excessive DC voltage u_f. The overvoltage protection induces a braking current i_{bk} as a function of i_{tot} and u_f, as described in the braking strategy (Fig. 3.a) [13]. All the braking current is therefore dissipated in the brake when the voltage $U_{ov\text{-}max}$ is reached. The braking coefficient k_{ov} decreases linearly from $U_{ov\text{-}min}$ to $U_{ov\text{-}max}$. The brake is represented by a current source, which imposes the current i_{bk} (2). As a static model of the input filter (inductor and DC bus) is used [17], the train current i_t is calculated by (3). An equivalent resistor $R_{f\text{-}t}$ represents the losses in the input filter (4). The EMR of the conventional train model is shown on Fig. 3.a. More details are available in [17].

$$i_{bk} = \begin{cases} 0 & \text{in traction mode} \\ (k_{ov} - 1).\, i_{tot} & \text{in braking mode} \end{cases} \tag{2}$$

$$\begin{cases} u_f & \text{common} \\ i_t = i_{tot} + i_{bk} \end{cases} \tag{3}$$

$$u_f = u_t - R_{f-t}.\, i_t \tag{4}$$

A new model has recently been proposed in [15]. It is based on a switched model of the rheostatic brake (Fig. 3.b), which is deduced from the overvoltage protection curve (Fig. 3.a).

1 – Brake off: When the brake is not activated, the train current i_t is i_{tot} (5) and the DC bus voltage u_f is determined by (4).

$$i_t = i_{tot} \tag{5}$$

2 – Brake on: When the brake is activated, it is considered as a voltage source, which imposes the maximum voltage $U_{ov\text{-}max}$, in series with an equivalent variable resistor r_{ov}. The DC bus voltage u_f and the train current i_t are determined respectively by (6) and (7). The brake current i_{bk} can be deduced by (8).

The switching conditions $C_{t\text{-}12}$ and $C_{t\text{-}21}$ of the models are given in Fig. 3.b and (9). More details are available in [15].

$$u_f = U_{ov-max} - r_{ov}.i_t \quad \text{with} \quad r_{ov} = \frac{U_{ov-max} - U_{ov-min}}{i_{tot}} \tag{6}$$

$$i_t = \frac{U_{ov-max} - u_t}{r_{eq-t}} \quad \text{with} \quad r_{eq-t} = r_{ov} - R_{f-t} \tag{7}$$

$$i_{bk} = i_t - i_{tot} \quad \text{and} \quad i_{bk-eq} = \frac{u_f}{U_{ov-max}}.i_{bk} \tag{8}$$

$$\begin{aligned} C_{t-12} &= \{i_{tot} < 0 \ \text{ AND } \ u_f \geq U_{ov-min}\} \\ C_{t-21} &= \{i_{tot} \geq 0 \ \text{ OR } \ u_f < U_{ov-min}\} \end{aligned} \tag{9}$$

B. *Model of the conventional TPS*

A conventional TPS consists of a transformer and a rectifier to convert the energy from the ACDN to the DCTN (Fig. 4). In this paper a 6-pulses diode rectifier is considered. But the proposed approach can be extended for other types of rectifiers.

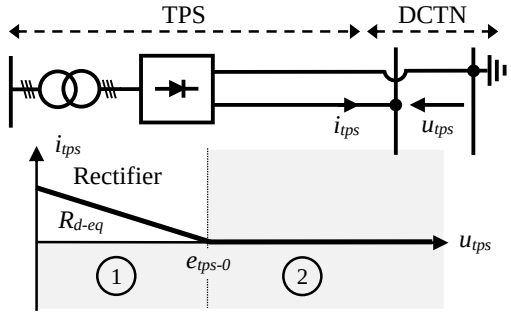

Fig. 4. Conventional non-reversible TPS.

In order to respect the interaction principle of the EMR, by considering an average model for the 3-phases AC part of the TPS, the formulation (10) has been chosen. The voltage variable v is 3 time the RMS value of the AC voltage. The current variable $\underline{i}$ is a vector composed of the RMS value of the AC current, the displacement angle φ between current and voltage, and the deformation angle γ due to harmonics. With this formulation, the product of the action variable with the reaction variable gives respectively the active P, reactive Q, and harmonics D powers (11). The total power S is given by (11).

$$v = 3.V_{rms} \quad \text{and} \quad \underline{i} = I_{rms}.\begin{bmatrix} \cos\varphi.\cos\gamma \\ \sin\varphi.\cos\gamma \\ \sin\gamma \end{bmatrix} \tag{10}$$

$$\begin{aligned} \begin{bmatrix} P \\ Q \\ D \end{bmatrix} &= v.\underline{i} = 3.V_{rms}.I_{rms}.\begin{bmatrix} \cos\varphi.\cos\gamma \\ \sin\varphi.\cos\gamma \\ \sin\gamma \end{bmatrix} \\ S &= 3.V_{rms}.I_{rms} = \sqrt{P^2+Q^2+D^2} \end{aligned} \tag{11}$$

The ACDN is represented as a voltage source v_g (12) (Fig. 5). A conventional model for the transformer is considered. It is composed of a resistor R_{ir} (iron losses) and a magnetizing inductor L_M on the primary side, and a resistor R_J (Joules losses) and a leakage inductor L_k on the secondary side. An ideal conversion factor $m_{p/s}$ is considered between the secondary and the primary windings. The current $\underline{i_g}$, imposed by the TPS on the ACDN, is therefore given by (12), with $\underline{i_{p\text{-}0}}$ the no-load current absorbed by R_{ir} and L_M (13), and $\underline{i_{s\text{-}2}}$ the current absorbed by the rectifier on the secondary of the transformer. The ideal voltage $v_{s\text{-}20}$ on the secondary is given by (14).

$$v_g = 3.V_{g-rms} \quad \text{and} \quad \underline{i_g} = \underline{i_{p-0}} + m_{p/s}.\underline{i_{s-2}} \tag{12}$$

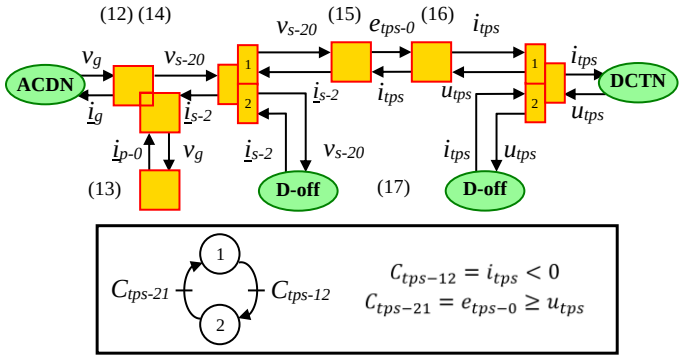

Fig. 5. EMR of the conventional non-reversible rectifier-based TPS.

$$\begin{cases} I_{p-0-rms} = \dfrac{\sqrt{R_{ir}^2 + (L_M.\omega_g)^2}}{R_{ir}.(L_M.\omega_g)}.V_{g-rms} \\ \varphi_{p-0} = \tan^{-1}\left(\dfrac{R_{ir}}{L_M.\omega_g}\right) \quad \text{and} \quad \gamma_{p-0} = 0 \end{cases} \tag{13}$$

$$v_{s-20} = m_{p/s}.v_g \tag{14}$$

A switched model is considered to represent the non-linear behavior of the diode rectifier (Fig. 5).

1 – Rectifier on-state: When the rectifier is on-state, it allows a power flow from the ACDN to the DCTN. It thus imposes the no-load DC voltage $e_{tps\text{-}0}$ on the DCTN (15). The RMS value and the displacement and deformation factors of the current $i_{s\text{-}2}$ are deduced from the DC current i_{tps} supplied by the TPS (15). The current i_{tps} is defined by (16), where $R_{d\text{-}eq}$ represents the voltage drop caused by the resistor R_J and by the overlap periods of the diodes of the rectifier due to the inductor L_k (see Fig. 4).

$$\begin{cases} e_{tps-0} = \dfrac{\sqrt{6}}{\pi}.v_{s-20} \quad \text{and} \quad I_{s-2-rms} = \sqrt{\dfrac{2}{3}}.i_{tps} \\ \varphi_{s-2} = \sin^{-1}\left(3.\dfrac{L_k.\omega_g}{v_{s-20}}.I_{s-2-rms}\right) \ \text{and} \ \gamma_{s-2} = \cos^{-1}\left(\dfrac{3}{\pi}\right) \end{cases} \tag{15}$$

$$i_{tps} = \frac{e_{tps-0} - u_{tps}}{R_{d-eq}} \quad \text{with} \quad R_{d-eq} = 2.R_J + \frac{3.L_k.\omega_g}{\pi} \tag{16}$$

2 – Rectifier off-state: When the rectifier is off-state, it is not possible to have a power flow from the DCTN to the ACDN. Consequently, the AC and DC currents are zero (17).

$$i_{tps} = 0 \quad \text{and} \quad \underline{i_{s-2}} = \begin{bmatrix} 0 \\ 0 \\ 0 \end{bmatrix} \tag{17}$$

The switching conditions $C_{tps\text{-}12}$ and $C_{tps\text{-}21}$ of the models are given in Fig. 5. More details are available in [14].

C. *Model of the reversible TPS*

The reversible TPS consists in a transformer and a combination of a rectifier and a controllable inverter (Fig. 6.a) [6]-[8]. There are other types of reversible TPS but they are not studied here. The rectifier realizes the positive power flow from the ACDN to the DCTN while the inverter is used to recover braking energy from the DCTN to the ACDN, thereby reducing the energy consumption of the entire railway system. Generally, the inverter control consists in imposing a negative current

according to the DC voltage level when the rectifier is blocked (Fig. 6.b) [6]-[8]. A voltage drop control with the slope $R_{1\text{-}eq}$ is considered. In this case, the inverter recovers energy when the voltage is greater than $U_{tps\text{-}1}$. It is also possible to take into account the minimum current $I_{tps\text{-}min}$ and power $P_{tps\text{-}min}$ limitations, which are reached when the voltage exceeds $U_{tps\text{-}max}$. A dead zone can be used between $e_{tps\text{-}0}$ (no-load DC voltage imposed by the rectifier) and $U_{tps\text{-}1}$. The slope of the drop control can be more or less important depending on the system capability and the possible and researched voltage control accuracy. Although the association of the inverter, the inductor $L_{f\text{-}tps}$, and its control can be considered as a controlled current source, another switched model is proposed to represent the different linear parts of the rectifier/inverter association. Therefore, four different models are developed for the four zones of the TPS operation (Fig. 6). The EMR and the switching conditions of the models are presented (Fig. 7).

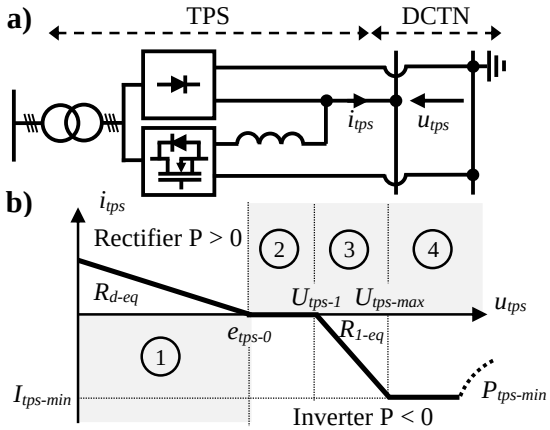

Fig. 6. Reversible TPS: a) Strucutre, b) Operations.

1 – Rectifier on-state (P > 0): When the rectifier is on-state ($e_{tps\text{-}0} \geq u_{tps}$), it supplies the DCTN as described for the conventional TPS (15) (16). The inverter is not used. The model of the reversible TPS is identical to that described previously.

2 – Rectifier off-state and inverter in dead zone (P = 0): In this operating zone ($e_{tps\text{-}0} > u_{tps} > U_{tps\text{-}1}$), the reversible TPS is a current source which imposes a zero current (18).

$$i_{tps} = 0 \tag{18}$$

3 – Rectifier off-state and inverter in voltage drop control (P < 0): In this operating zone ($U_{tps\text{-}1} \geq u_{tps} > U_{tps\text{-}max}$), the rectifier is blocked, and the inverter operates under voltage drop control. The reversible TPS is considered as a voltage source $U_{tps\text{-}1}$ in series with a resistor $R_{1\text{-}eq}$. The current is given by (19).

$$i_{tps} = \frac{U_{tps-1} - u_{tps}}{R_{1-eq}} \text{ with } R_{1-eq} = \frac{U_{tps-1} - U_{tps-max}}{I_{tps-min}} \tag{19}$$

4 – Rectifier off-state and inverter in current limitation (P < 0): In this operating zone ($U_{tps\text{-}max} < u_{tps}$), the rectifier is still blocked, and the inverter recovers the current $I_{tps\text{-}min}$ from the DCTN to the ACDN. It is a current source (20).

$$i_{tps} = I_{tps-min} \tag{20}$$

With models 2, 3 and 4, the active power p_{inv} of the inverter is determined by (21), with R_L the Joules losses in the inductor $L_{f\text{-}tps}$, and n_{inv} the efficiency of the inverter. The power factor control function of such inverters allows the control of the reactive power q_{inv} (in this paper, it will be set to zero). In addition, the power q_{inv} of the harmonics is considered to be close to zero due to the pulse width modulation techniques of such inverters. The total power s_{inv} is thus determined in (21).

$$\begin{aligned} p_{inv} &= \frac{u_{tps}.i_{tps} + R_L.{i_{tps}}^2}{n_{inv}^k} \text{ with } k = \begin{cases} 1 & \text{when } P > 0 \\ -1 & \text{when } P < 0 \end{cases} \\ q_{inv} &= Q_{inv-ref} = 0 \quad \text{and} \quad d_{inv} = 0 \\ s_{inv} &= \sqrt{{p_{inv}}^2 + {q_{inv}}^2 + {d_{inv}}^2} \end{aligned} \tag{21}$$

The resolution of the second order equation (22) allows the determination of the current variable $\underline{i}_{s\text{-}2}$ at the secondary of the transformer, with $I_{s\text{-}2\text{-}rms}$ the RMS value of the current, $\varphi_{s\text{-}2}$ the displacement angle φ between the current and the voltage, and $\gamma_{s\text{-}2}$ the deformation angle due to harmonics (zero in this case).

$$\begin{cases} s_{inv} = v_{s-20}.I_{s-2-rms} - 3.{I_{s-2-rms}}^2.\sqrt{{R_J}^2 + (L_k.\omega_g)^2} \\ \varphi_{s-2} = \sin^{-1}\left(\dfrac{q_{inv} + 3.L_k.\omega_g.{I_{s-2-rms}}^2}{v_{s-20}.I_{s-2-rms}}\right) \text{ and } \gamma_{s-2} = 0 \end{cases} \tag{22}$$

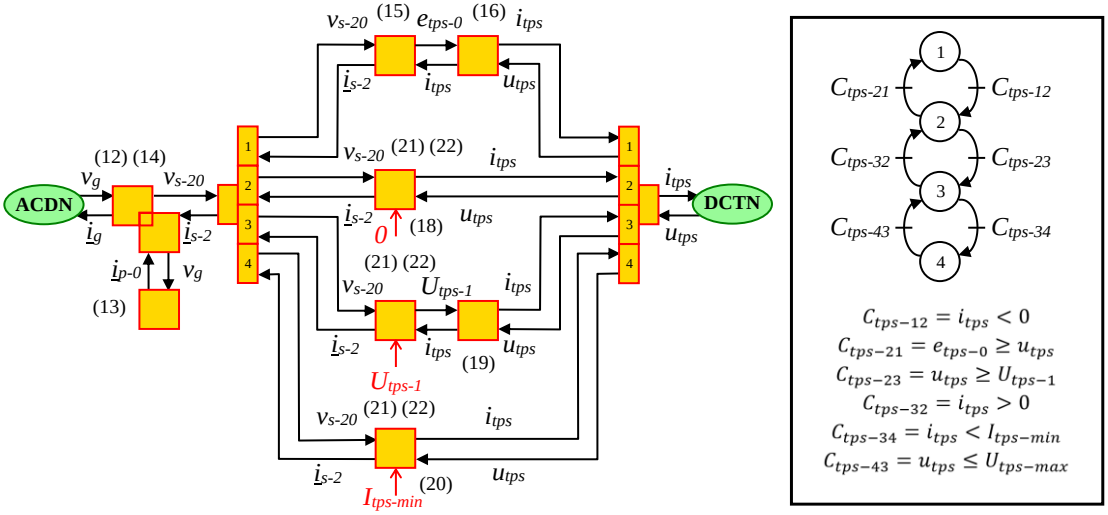

Fig. 7. EMR and switching contidions of the reversible TPS.

D. Model of the DCTN

The DCTN model assumes a linear resistance distribution along the line. A dedicated methodology based on the Modified Nodal Analysis is used. More information is available in [15].

III. DC Railway Simulation

Coupling the models of the different subsystems gives the complete simulation model of the DC railway system. This section will be described in the final paper with the description of the EMR and the solving procedure (with the MNA).

IV. Simulation Results

The test line is derived from an existing conventional light rail system described in [13]. But only the first 6.9 km of the line are considered in this paper (8 passenger stations and 3 TPS) for simplicity reason. All the data is in [13]. The simulation is performed with a headway between the train of 520 s, which requires 4 trains on the line. The simulation results are obtained for two cases: with non-reversible TPS and with reversible TPS. The overvoltage protection is activated between 900 V ($U_{ov\text{-}min}$) and 950 V ($U_{ov\text{-}max}$). The no-load rectifier voltage (e_{ss0}) is equal to 750 V. Reversible TPS recover energy between 800 V ($U_{tps\text{-}1}$) and 850 V ($U_{tps\text{-}max}$) using the voltage drop control. They absorb the minimum current ($I_{tps\text{-}min}$ = -200 A) above 850 V. The power limitation is not used in this paper. The results (Fig. 8) present the total energy and the total active power on the ACDN (for the 3 TPS), as well as the DC current i_{tps} and voltage u_{tps} of TPS 2. The results highlight that reversible TPS allow an energy saving of around 7 % on total energy consumption compared to conventional TPS in the studied case. In addition, the use of reversible TPS improves the voltage stabilization of the DCTN. More results and analysis will be provided in the final paper.

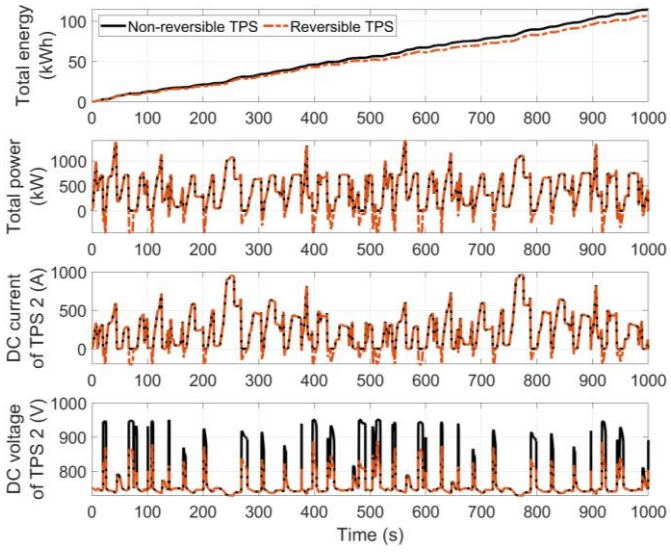

Fig. 8. Simulation results.

V. Conclusion

The paper presents a method for modeling and simulating complete DC railway systems. Switched models are used for the different subsystems in order to take into account their non-linearities and limitations. A complete methodology is presented based on the Energetic Macroscopic Representation (EMR). The methodology is applied to a light rail system with conventional non-reversible Traction Power Substation (TPS) but also with reversible TPS. The energy saving is estimated for a specific scenario. Reversible TPS allow an energy reduction of 7 %.

References

[1] C. C. Chan, "Overview of electric, hybrid, and fuel cell vehicles," *Encyclopedia of Autom. Eng.*, Hoboken, NJ, USA: Wilez, ch 51, 2015.

[2] R. Barrero, J. van. Mierlo, and X. Tackoen, "Energy savings in public transport," *IEEE Veh. Technol. Mag.*, vol. 3, no. 3, pp. 26–36, Sep. 2008.

[3] L. Alfieri, L. Battistelli, and M. Pagano, "Impact on railway infrastructure of wayside energy storage systems for regenerative braking management: a case study on a real Italian railway infrastructure," *IET Electr. Syst. Transp.*, vol. 9, no. 3, pp. 140–149, Sep. 2019.

[4] M. Khodaparastan, O. Dutta, M. Saleh, and A. A. Mohamed, "Modeling and simulation of DC electric rail transit systems with wayside energy storage," *IEEE Trans. Veh. Technol.*, vol. 68, no. 3, pp. 2218–2228, Mar. 2019.

[5] R. Takagi, and T. Amano, "Optimization of reference state-of-charge curves for the feed-forward charge/discharge control of energy storage systems on-board DC electric railway vehicles," *IET Electr. Syst. Transp.*, vol. 5, no. 1, pp. 33–42, Feb. 2015.

[6] P. Arboleya, B. Mohamed, and I. El-Sayed, "DC railway simulation including controllable power electronic and energy storage devices," *IEEE Trans. Power Syst.*, vol. 33, no. 5, pp. 5319–5329, Feb. 2018.

[7] V. A. Kleftakis, and N. D. Hatziargyriou, "Optimal control of reversible substation and wayside storage devices for voltage stabilization and energy savings in metro railway networks," *IEEE Trans. Transp. Electrific.*, vol. 5, no. 2, pp. 515–523, Apr. 2019.

[8] G. Zhang, Z. Tian, P. Tricoli, S. Hillmansen, Y. Wang and Z. Liu, "Inverter operating characteristics optimization for DC traction power supply systems," *IEEE Trans. Veh. Technol.*, vol. 68, no. 4, pp. 3400–3410, Apr. 2019.

[9] R.-J. Jabr, and I. Dzafic, "Solution of DC railway traction power flow systems including limited network receptivity," *IEEE Trans. Power Syst.*, vol. 33, no. 1, pp. 962–969, Mar. 2017.

[10] B. Ku, and J. Liu, "Modelling and numerical solution of undergrounded DC rail traction system load flow using a Ladder circuit – Part I: circuit modelling," *IET Generation, Transmission & Distribution.*, vol. 14, no. 1, pp. 1–10, Jan. 2020.

[11] C.-W. Ho, A. Ruehli, and P. Brennan, "The modified nodal approach to network analysis," *IEEE Trans. Circuits Syst.*, vol. 22, no. 6, pp. 504–509, Jun. 1975.

[12] V. Acary, O. Bonnefon, and B. Brogliato, "Nonsmooth modelling and simulation of switched circuits," *Springer Science & Business Media*, 2010.

[13] C. Mayet, A. Bouscayrol, P. Delarue, E. Chattot, and J.-N. Verhille, "Electrokinematical simulation for flexible energetic studies of railway systems," *IEEE Trans. Ind. Electron.*, vol. 65, no. 4, pp. 3592–3600, Apr. 2018.

[14] C. Mayet, P. Delarue, A. Bouscayrol, E. Chattot, and J.-N. Verhille, "Comparison of different EMR-based models of Traction Power Substations for energetic studies of subway lines," *IEEE Trans. Veh. Technol.*, vol. 65, no. 3, pp. 1021–1029, Mar. 2016.

[15] C. Mayet, P. Arboleya, A. Bouscayrol, B. Mohamed, P. Delarue, I. El-Sayed, "Non-linear switched model for accurate voltage estimation and power flow analysis of DC railway systems, *IET Electr. Syst. Transp.*, Jun. 2020 (accepted).

[16] A. Bouscayrol, J.-P. Hautier, and B. Lemaire-Semail, "Systemic design methodologies for electrical energy systems – Chapter 3: Graphic formalism for the control of multi-physical energetic systems: COG and EMR," *ISTE Ltd and John Wiley & Sons, Inc.*, 2012.

[17] C. Mayet, L. Horrein, A. Bouscayrol, P. Delarue, J.-N. Verhille, E. Chattot, and B. Lemaire-Semail, "Comparison of different models and simulation approaches for the energetic study of a subway," *IEEE Trans. Veh. Technol.*, vol. 63, no. 2, pp. 556–565, Feb. 2014.